THE JOURNAL OF PHYSICAL CHEMISTRY C

Article

pubs.acs.org/JPCC

Direct Observation of Active Nickel Oxide Cluster in Nickel–Borate Electrocatalyst for Water Oxidation by In Situ O K-Edge X-ray Absorption Spectroscopy

Masaaki Yoshida,*[,†,‡] Yosuke Mitsutomi,[†] Takehiro Mineo,[†] Masanari Nagasaka,[§] Hayato Yuzawa,[§] Nobuhiro Kosugi,[§] and Hiroshi Kondoh[†]

[†]Department of Chemistry, Keio University, 3-14-1 Hiyoshi, Kohoku-ku, Yokohama 223-8522, Japan

[‡]Cooperative Research Fellow, Catalysis Research Center, Hokkaido University, Kita21, Nishi10, Kita-ku, Sapporo, Hokkaido 001-0021, Japan

[§]Institute for Molecular Science, 38 Nishigo-Naka, Myodaiji, Okazaki 444-8585, Japan

Supporting Information

ABSTRACT: In situ O K-edge X-ray absorption fine structure (XAFS) spectroscopy was applied to investigate the electronic and structural change in the nickel–borate (Ni–B_i) electrocatalyst during the oxygen evolution reaction (OER). An absorption peak was observed around 528.7 eV at 1.0 V versus Ag/AgCl in a potassium borate aqueous solution, which relates with the formation of nanoscale order domains of edge-sharing NiO_6 octahedra in the Ni–B_i electrocatalyst. XAFS spectra were measured with variation of the electrode potential from 0.3 up to 1.0 V. The measured absorption peaks suggest that the quantity of NiO_6 octahedra increased in correlation with the OER current; however, when the potential was changed downward, the XAFS absorption peak assigned to NiO_6 octahedra remained constant, even at the electrode potential for no OER current. This difference implies that the water oxidation catalysis proceeds at the domain edge of NiO_6 octahedra. The XAFS technique provides the first successful direct probing of the active species in the Ni–B_i electrocatalyst during electrochemical reaction.

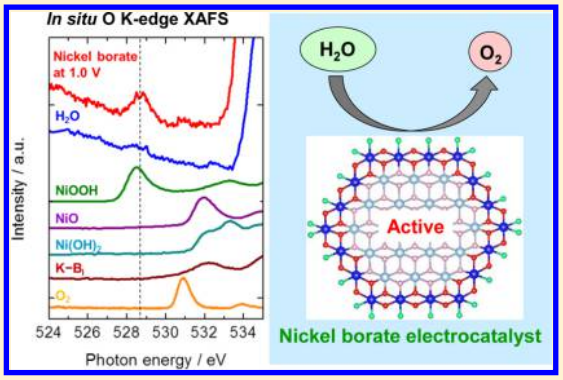

1. INTRODUCTION

Water splitting using solar energy is a promising approach to produce renewable hydrogen gas toward a sustainable society.[1−7] Various types of photoelectrodes and photovoltaics for water splitting have been developed with high solar-to-hydrogen efficiencies of over several percent.[8−12] Recently, a perovskite photovoltaic attained a solar-to-hydrogen efficiency of 12.3% using hydrogen and oxygen evolution electrocatalysts.[8] For the realization of efficient photovoltaic and photoelectrochemical systems for water splitting, oxygen evolution catalysts have often been used to catalyze water oxidation due to their lower activation energies. Therefore, the development of efficient catalysts for the oxygen evolution reaction (OER) has attracted considerable attention due to the potential toward highly efficient energy conversion.

Nocera and colleagues reported that nickel–borate electrodeposited from a dilute Ni^{2+} solution in a borate-buffered electrolyte (Ni–B_i) functions as an efficient OER electrocatalyst.[13−15] The Ni–B_i OER catalyst is unique because it is composed of inexpensive and earth-abundant materials, and it operates safely with high activity.[13−15] As similar materials, cobalt–phosphate (Co–P_i) and cobalt–borate (Co–B_i) complexes have also been reported as efficient electrocatalysts for OER in phosphate and borate electrolytes, respectively.[16−19] These OER electrocatalysts can enhance the activities for water splitting, when the electrocatalysts are deposited on a semiconductor photoelectrode or photovoltaic surfaces such as Si, Fe_2O_3, and $BiVO_4$.[9,11,20−23]

Mechanistic studies that employ various techniques have been aimed toward determining the origin of efficient oxygen evolution for Ni–B_i electrocatalysts or similar materials (Co–P_i, Co–B_i).[24−35] An electron paramagnetic resonance (EPR) spectroscopy study revealed the presence of Co^{4+} species in a Co–P_i electrocatalyst in a frozen electrolysis solution.[35] In addition, Ni K-edge X-ray absorption fine structure (XAFS) analysis demonstrated that the average valence state of the nickel species in a Ni–B_i electrocatalyst changes from +2.0 to +3.6 in response to an applied positive voltage.[24] It was concluded that oxidation of the nickel species is due to the generation of bis-oxo/hydroxo-bridged nickel centers organized into sheets of edge-sharing NiO_6 octahedra within ordered domains 2 to 3 nm in diameter by extended X-ray absorption fine structure (EXAFS) analysis.[24] The nanoscale order structures of the Co–P_i and Co–B_i electrocatalysts were

Received: June 25, 2015
Revised: July 31, 2015
Published: July 31, 2015

DOI: 10.1021/acs.jpcc.5b06102
J. Phys. Chem. C 2015, 119, 19279−19286

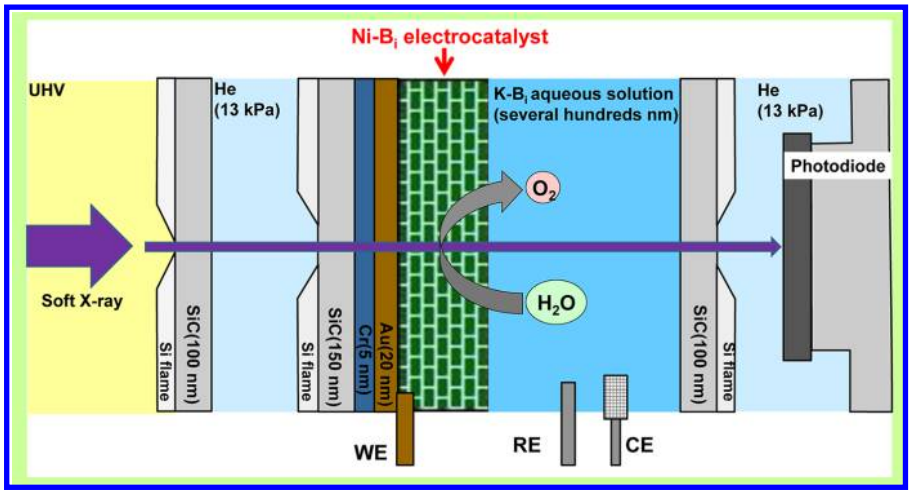

Figure 1. Schematic illustration of optical geometry for in situ O K-edge XAFS measurements with the transmission mode at the BL3U beamline. A liquid layer of several hundreds of nanometers was sandwiched between the SiC and Au/Cr/SiC membranes by setting Teflon and Au spacers (100 μm thickness) to the window frames of the membranes in an in house-built electrochemical XAFS cell with Pt mesh counter and Ag/AgCl (saturated KCl) reference electrodes. The potential of the Au/Cr/SiC working electrode was controlled using a potentiostat connected to the Au spacer with a conducting wire.

investigated by X-ray pair distribution function (PDF) analysis[32,33] and a combination study using infrared spectroscopy (IR), atomic force microscopy (AFM), and X-ray grazing incidence diffraction (GID),[34] from which it was determined that nanoscale CoO_6 clusters can assemble into stacked superstructures with highly porous morphology. It is suggested that the porous electrocatalyst film enables proton-coupled electron hopping to proceed in the electrocatalyst, which can increase the OER sites with growth of the film thickness.[28,30] Therefore, the unique characteristics of these electrocatalysts are currently of particular interest as a material for efficient OER.

XAFS spectroscopy is a powerful tool to investigate the local electronic states for OER catalysts.[24,25,36,37] The in situ Ni K-edge XAFS technique using hard X-rays was applied to the Ni–B$_i$ electrocatalyst; however, it is difficult to quantitatively discuss the active species in the OER electrode potential with this technique because the Ni K-edge XAFS spectra become a superposition of each spectrum for Ni^{2+} and $Ni^{3.6+}$ species in the Ni–B$_i$ electrocatalyst and Ni^{2+} cations in the electrolyte solution.[24,36] On the contrary, O K-edge XAFS spectroscopy using soft X-rays has been useful to directly observe the oxygen species in transition-metal oxides at the liquid/solid interface.[38,39] Therefore, in this study, the Ni–B$_i$ electrocatalyst was investigated using in situ O K-edge XAFS measurements with control of the potential. An attempt was made to directly detect the active oxygen species in the Ni–B$_i$ electrocatalyst and discuss the relationship between the amount of active species and the OER activity.

2. EXPERIMENTAL SECTION

2.1. Sample Preparation. Au thin films (20 nm) were deposited on Si substrates (10 × 10 mm^2) with an evaporated Cr layer (5 nm thick) and SiC (150 nm thick, 2 × 2 mm^2, NTT AT) or Si_3N_4 (500 nm thickness, 2 × 2 mm^2, CORNES Technologies) windows (Au/Cr/SiC or Au/Cr/Si_3N_4, respectively) for use as working electrodes for electrochemical reactions. An in-house-built electrochemical cell was used with a Pt mesh counter electrode and a Ag/AgCl (saturated KCl) reference electrode. The potential was controlled using a potentiostat. A Ni–B$_i$ electrocatalyst was deposited on the Au thin film electrodes in 0.1 M $K_2B_4O_7{\cdot}4H_2O$ (potassium borate, K–B$_i$, 99.0%, Showa Chemical) aqueous solution containing 0.4 mM $Ni(NO_3)_2$ (99.9%, Wako Pure Chemical Industries) with bubbling He, according to a previous report.[24] Milli-Q water (total organic carbon <5 ppb, resistivity >18 MΩ·cm) was used for all experiments. The electrochemical activity of the Ni–B$_i$ electrocatalyst for the OER was tested in K–B$_i$ aqueous solution with bubbling He by measurement of the current–voltage characteristics. The surface morphology, chemical state, and film thickness of each prepared sample were observed using scanning electron microscopy (SEM; FEI, Inspect S50), energy-dispersive X-ray spectroscopy (EDX; EDAX, Genesis), and confocal laser scanning microscopy (CLSM; Keyence, VK-9710), respectively.

2.2. In situ O K-Edge XAFS. Electrochemical soft X-ray XAFS measurements were performed with the transmission mode at the BL3U beamline of the UVSOR Synchrotron, in accordance with previous work.[40,41] The radiation was monochromatized with a varied-line-spacing plane-grating monochromator (VLS-PGM). The intensities of the incident X-rays were monitored using a gold mesh under ultrahigh vacuum in front of the sample (I_0) and a photodiode (IRD AXUV100) under a helium atmosphere after the sample (I_1). The XAFS data were collected as transmission spectra with the Lambert–Beer formula $\ln(I_0/I_1)$. The photon energy was calibrated according to the O 1s–π^* peak (530.80 eV)[42] for O_2 gas mixed in a buffer gas with He gas. The O K-edge XAFS spectrum of Milli-Q water was measured as a reference sample for sample sandwiched between two SiC membranes (100 nm thickness, 2 × 2 mm^2, NTT AT). On the contrary, the O K-edge XAFS spectra for the $Ni(OH)_2$, NiO, β–NiOOH, and K–B$_i$ reference samples were obtained by measuring the sample drain current under ultrahigh vacuum. For the investigation of electrochemical reactions, we sandwiched a liquid layer of a several hundreds of nanometers between the SiC and Au/Cr/SiC membranes by setting Teflon and Au spacers (100 μm thickness) to the window frames of the membranes in an in-house-built electrochemical XAFS cell with a Pt mesh counter and Ag/AgCl (saturated KCl) reference electrodes (Figure 1).

DOI: 10.1021/acs.jpcc.5b06102
J. Phys. Chem. C 2015, 119, 19279–19286

The electrolyte thickness was adjusted by changing the outer helium gas pressure of the SiC and Au/Cr/SiC membranes, according to the previous works.[40,41] The potential of the Au/Cr/SiC working electrode was controlled using a potentiostat connected to the Au spacer with a conducting wire. The Ni−B_i electrocatalyst was deposited on the Au thin film electrode in 0.1 M K−B_i aqueous solution containing 0.4 mM $Ni(NO_3)_2$ with bubbling He. The Ni−B_i electrocatalyst was then anodized at 1.0 V for 2 h in 0.5 M K−B_i aqueous solution with bubbling He by exchanging the solutions with a tubing pump system. In situ O K-edge XAFS spectra were measured for the Ni−B_i electrocatalyst before and after anodization while maintaining the electrode potential at 1.0 V. The potential dependence of the XAFS spectra was tested in 0.1 M K−B_i aqueous solution with bubbling He by exchanging solutions with the tubing pumping system during current monitoring for the OER with the potentiostat. The XAFS spectra were taken with scanning time of 20 min at cumulated number of 3 times, which results in each electrode potential being applied for 1 h.

3. RESULTS AND DISCUSSION

3.1. Electrochemical Properties and Surface Morphologies. The current during electrodeposition of the Ni−B_i electrocatalyst increased for 2 h, as shown in Figure S1a, which indicates growth of the Ni−B_i thin film and the evolution of oxygen gas not only at the Ni−B_i surface but also from the Ni−B_i interior, as previously reported.[13−15,24,28,30] The anodization reaction of the Ni−B_i electrocatalyst was monitored, as shown in Figure S1b, and the current continued to increase for 2 h as in the previous work.[24] Figure 2a shows the electrochemical

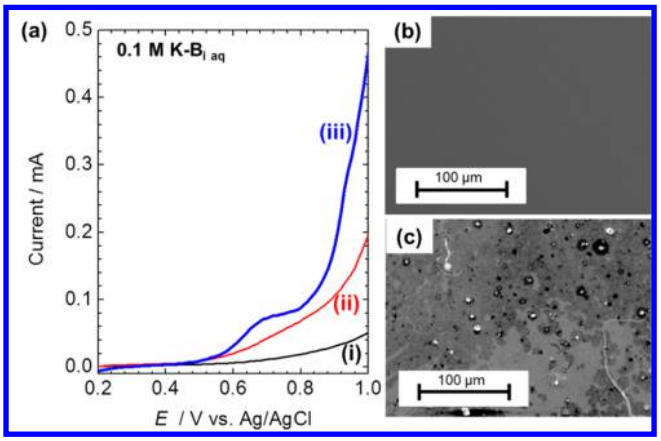

Figure 2. (a) Current−voltage characteristics for (i) bare (black) and (ii,iii) Ni−B_i-modified (nonanodized; red and anodized; blue) Au thin films in a 0.1 M K−B_i aqueous electrolyte. SEM images of the Au thin film (b) before and (c) after the electrodeposition of Ni−B_i.

OER activities of the prepared samples, where the efficiency of the Ni−B_i-deposited substrate was higher than that of the bare substrate; therefore, the Ni−B_i thin film functions as an OER electrocatalyst. In addition, the current of the anodized sample was higher than that of the nonanodized sample, which indicates that anodization of the Ni−B_i electrocatalyst enhances the OER activity, in agreement with the previous report.[24] It should be noted that the oxidation currents for nonanodized and anodized samples were both observed around 0.7 V because the nickel species in the nonanodized or anodized Ni−B_i electrocatalyst was oxidized from $Ni(OH)_2$ (Ni^{2+}) to β-NiOOH (Ni^{3+}) or to γ-NiOOH ($Ni^{3.6+}$), respectively (See the next Discussion). Figure 2b,c shows SEM images of the Au/Cr/SiC substrate before and after Ni−B_i electrodeposition and confirms that the Ni species was deposited on the substrate as a thin film. SEM-EDX analysis confirmed that the observed thin film was composed of Ni−B_i electrocatalyst as well as the previous work.[13] The film thickness was estimated to be ca. 300 nm by the CLSM method (Figure S2).

3.2. In situ O K-Edge XAFS. Figure 3a shows an in situ O K-edge XAFS spectrum measured for the electrodeposition

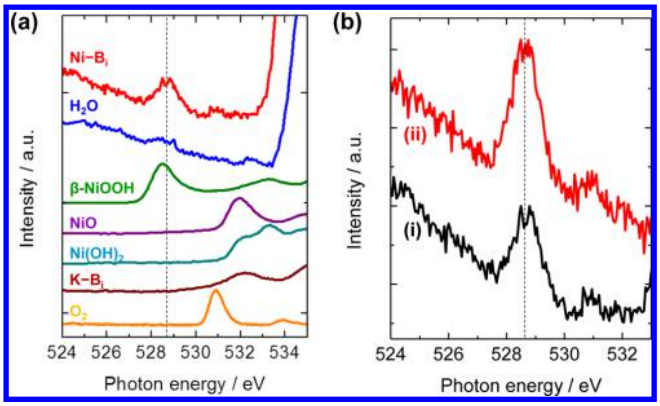

Figure 3. (a) In situ O K-edge XAFS spectrum for Ni−B_i electrocatalyst under electrochemical control at 1.0 V in 0.1 M K−B_i aqueous solution containing 0.40 mM $Ni(NO_3)_2$. XAFS spectra for H_2O, β−NiOOH, NiO, $Ni(OH)_2$, K−B_i, and O_2 gas are shown for reference. (b) In situ O K-edge XAFS spectra (i) before and (ii) after anodization for 2 h at 1.0 V in 0.5 M K−B_i aqueous solution.

reaction of Ni−B_i thin film at 1.0 V versus Ag/AgCl in a 0.1 M K−B_i aqueous solution containing 0.4 mM $Ni(NO_3)_2$, together with those for H_2O, β-NiOOH, NiO, $Ni(OH)_2$, K−B_i, and O_2 gas as references that relate with the Ni−B_i catalysis. A peak associated with an oxygen species was observed at ca. 528.7 eV, which was similar to that in the β-NiOOH reference. To evaluate the electrode potential dependence of the Ni−B_i electrocatalyst, we changed the electrolyte solution to 0.5 M K−B_i aqueous solution without nickel ions, and we conducted XAFS measurements while changing the applied electrode potential. The peak at ca. 528.7 eV disappeared at the lower potential (0.5 V) and reappeared at the higher potential (1.0 V) accompanied by the OER activity, as shown in Figure 4a. The same behavior was observed even in 0.05 M K−B_i aqueous solution (Figure 4b). Previous Ni K-edge EXAFS measurements[24] suggested that the Ni−B_i electrocatalyst before anodization forms μ-oxo/hydroxo nickel centers organized into higher order domains of edge-sharing NiO_6 octahedra with β-NiOOH structure at higher potential. Thus, in the present study, the formation of NiO_6 octahedra domains can be monitored by the direct observation of oxygen species in the Ni−B_i thin film. The NiO_6 absorption was observed as a single peak at 528.7 eV, which originates from transition to hybridized Ni(3d)−O(2p) states with e_g orbital symmetry and the low-spin d7 (Ni^{3+}) electron configuration.[24] It should be noted that the small peak around 530.8 eV in Ni−B_i is attributed to the strong 1s-π^* resonance absorption of residual oxygen gas.[42] No detection of the $Ni(OH)_2$ peak at lower potential in the O K-edge spectra may be mostly because the electronic state of oxygen species of $Ni(OH)_2$ structure in the Ni−B_i electrocatalyst is not uniform due to hydration or protonation on the Ni−B_i film.

DOI: 10.1021/acs.jpcc.5b06102
J. Phys. Chem. C 2015, 119, 19279−19286

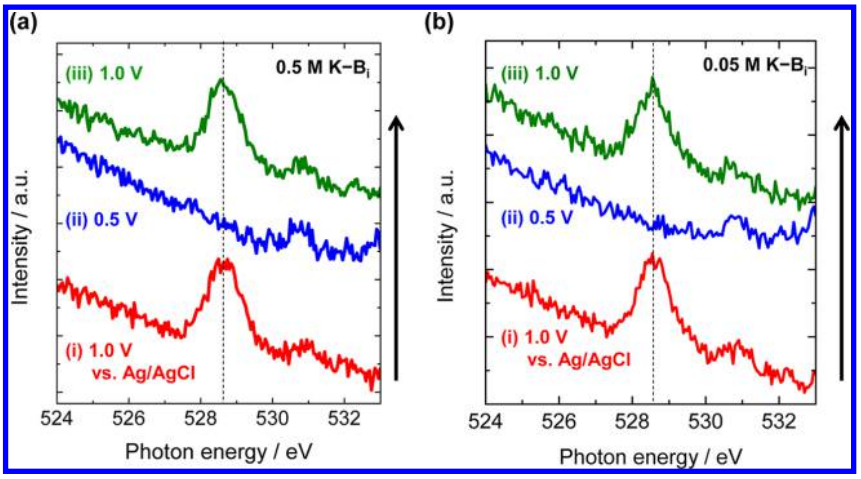

Figure 4. Potential dependence of in situ O K-edge XAFS spectra by changing the electrode potential at (i) 1.0, (ii) 0.5, and (iii) 1.0 V versus Ag/AgCl in (a) 0.5 M and (b) 0.05 M K–B_i aqueous electrolyte. The peak at ca. 528.7 eV measured at 1.0 V disappeared at the lower potential (0.5 V) and then reappeared at the higher potential (1.0 V) accompanied by OER activity.

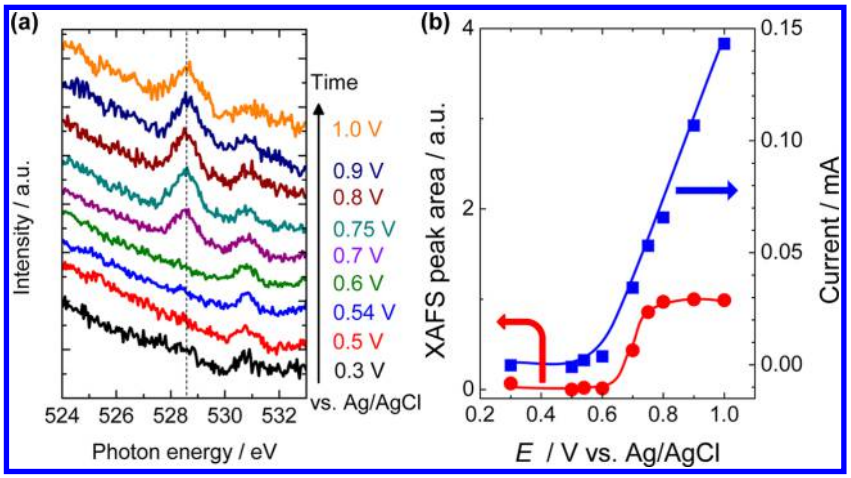

Figure 5. (a) Upward potential dependence of in situ O K-edge XAFS spectra for the Ni–B_i electrocatalyst in 0.1 M K–B_i aqueous solution from 0.3 to 1.0 V. (b) Relationship between XAFS peak area and current for the OER with respect to the electrode potential.

Anodization of the Ni–B_i electrocatalyst caused the NiO_6 octahedra peak to increase, as shown in Figure 3b. Bediako et al. reported that the inactive Ni–B_i species with β-NiOOH structure (Ni^{3+}) changed to the active Ni–B_i species with γ-NiOOH structure ($Ni^{3.6+}$), which resulted in the relaxation of Jahn–Teller distortion with nonequivalent Ni–O and Ni–Ni distances.[24] We also verified the existence of γ-NiOOH structure for our Ni–B_i sample by in situ Ni K-edge XAFS measurements as well as the previous work,[24] as shown in Figure S3. Both NiOOH structures have two kinds of oxygen species derived from hydroxide (OH) and oxide (O) at an different OH/O ratio (e.g., β–NiOOH = $Ni^{3+}(O)_1(OH)_1$, γ–NiOOH = $Ni^{3.6+}(O)_{1.6}(OH)_{0.4}$). It is known that the 1s core level of oxygen species of hydroxide (OH) is shifted to higher binding energy with respect to that of oxygen species of oxide (O) in transition-metal oxyhydroxides, which results in the oxide oxygen peak being observed at a lower energy than the hydroxide oxygen peak in the O K-edge XAFS spectra.[43] Thus, in the present work, the first peaks in the O K-edge XAFS spectra are likely attributed to the oxide oxygen species in the β- and γ-NiOOH structures, and the increase of the XAFS peak is most likely due to an increase in the oxide oxygen species by the structural change from β-NiOOH (Ni^{3+}) to γ-NiOOH ($Ni^{3.6+}$). On the contrary, the first peak positions in the O K-edge XAFS spectra for transition-metal oxides are empirically related with the cation valences to some extent.[44,45] Therefore, the local nickel valence bound by oxide oxygen species in the Ni–B_i electrocatalyst was tentatively estimated as ca. 4+ using the linear fitting of first peak positions of reference compounds against the cation valences, as shown in Figure S4, which suggests that the highly oxidized Ni species such as NiO_2 are formed during catalytic water oxidation. It should be noted that the O K-edge XAFS spectra are sensitive to chemical bonding (molecular orbitals), valence, spin state, and so on.[38,39,43−46] Further investigation is required to evaluate the cation valence quantitatively.

3.3. Electrode Potential Dependence of XAFS Spectra and Reaction Model. The upward potential dependence of the Ni–B_i electrocatalyst on the Au thin film was evaluated. Figure 5a shows O K-edge XAFS spectra for this sample measured under various controlled potentials. As the potential was changed from 0.3 to 1.0 V, the intensity of the peak for the NiO_6 octahedra increased from 0.6 V and remained constant over 0.8 V, which indicates that the nickel species was oxidized from Ni^{2+} species with the $Ni(OH)_2$ structure to NiO_6 octahedra on the basis of previous works.[24,36] The increase in

DOI: 10.1021/acs.jpcc.5b06102
J. Phys. Chem. C 2015, 119, 19279−19286

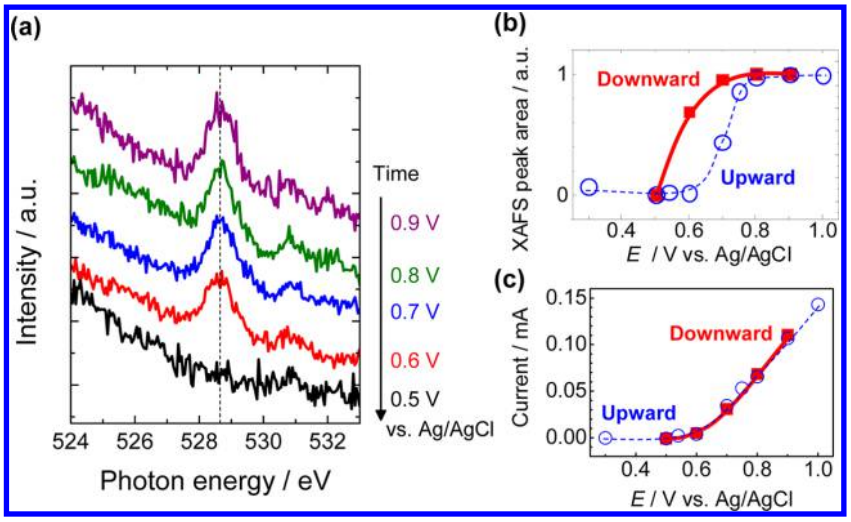

Figure 6. (a) Downward potential dependence of in situ O K-edge XAFS spectra for the Ni−B_i electrocatalyst in 0.1 M K−B_i aqueous solution from 0.9 to 0.5 V. (b) XAFS peak areas and (c) currents for the OER with respect to the electrode potential.

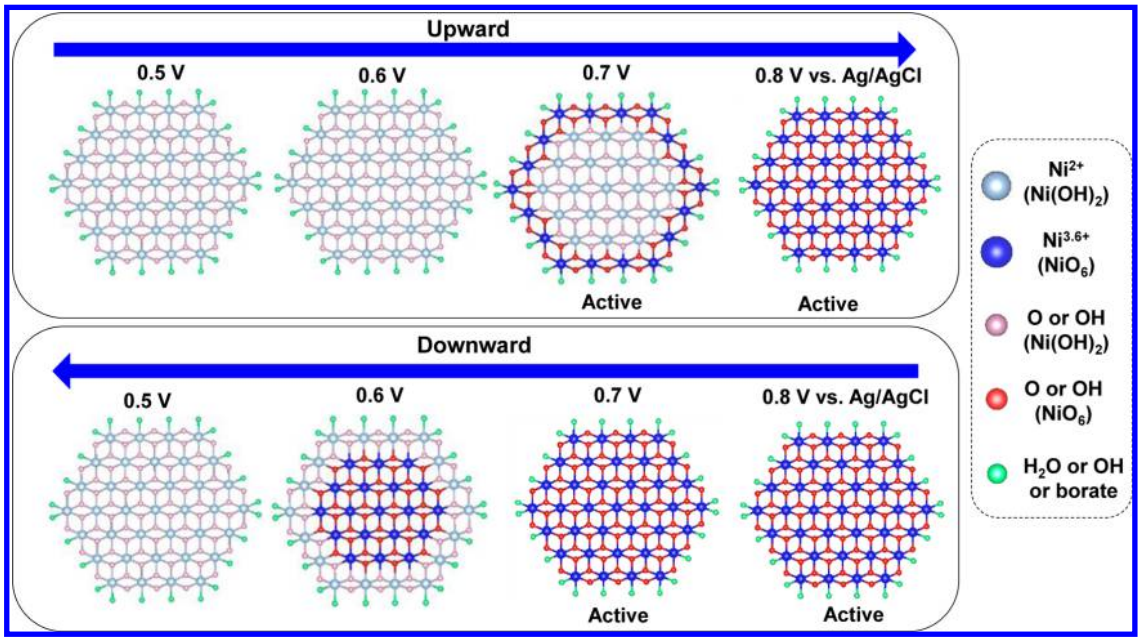

Figure 7. Schematic model for nickel oxide nanoclusters in the Ni−B_i electrocatalyst during OER catalysis in K−B_i aqueous solution with the electrode potential swept upward and downward. It should be noted that $Ni(OH)_2$ has an octahedral structure similar to NiO_6.[26,48]

the edge of XAFS peak area for NiO_6 octahedra was consistent with the onset of OER activity (Figure 5b), which indicates that the high activity of the Ni−B_i thin film for the OER is derived from the formation of NiO_6 octahedra domains. On the contrary, the XAFS peak remains constant at higher electrode potentials (≥0.8 V) because the nickel oxide nanoclusters were completely oxidized to NiO_6 octahedra. The increase in the OER current even in the suppression region of peak growing in XAFS spectra suggests that the reaction rate for OER catalysis at higher potentials is probably restricted according to the Tafel equation, relating the rate of an electrochemical reaction to the overpotential as $V = a + b \log I$, where V is the potential (overpotential), I is the current density, and a and b are the Tafel equation constants.[47]

To compare the difference according to the direction of potential sweep, we measured the downward potential dependence of XAFS spectra under potential control (Figure 6a). The NiO_6 XAFS peak at 528.7 eV was observed at higher potential as well as the result of upward potential dependence; however, the peak was observed even at 0.6 V, which indicates that the generated NiO_6 octahedra were not easily reduced to the Ni^{2+} species. The relationship between the electrode potential and XAFS peak area suggests that the downward potential dependence is different from that of the upward potential dependence, as shown in Figure 6b. The result indicates that the nickel oxide nanocluster was gradually reduced from the domain edge because the oxidation and reduction of domain edge is likely to proceed by lower activation energy than those of domain inside; however, the currents for OER activity were the same for the upward and downward sweeps (Figure 6c), which implies that the interior of the NiO_6 octahedra structure does not function as an OER site. Figure 7 shows a schematic model for water oxidation during upward and downward potential sweeps. The upward

DOI: 10.1021/acs.jpcc.5b06102
J. Phys. Chem. C 2015, 119, 19279−19286

potential change results in oxidation of the Ni^{2+} species with $Ni(OH)_2$ structure[48] to the $Ni^{3.6+}$ species with NiO_6 octahedra structure accompanied by OER activity. In contrast, the downward potential change gradually reduces the $Ni^{3.6+}$ species to Ni^{2+} from the domain edge and the OER activity is suppressed when the outer NiO_6 octahedra domain is reduced. On the basis of these results, water oxidation is likely to proceed at the domain edge of NiO_6 octahedra.

Reaction pathways for OER catalysis with Ni−B_i, Co−B_i, and Co−P_i electrocatalysts were previously proposed.[24−35] Bediako et al. elucidated that the OER over the Ni−B_i electrocatalyst in borate-buffered electrolyte entails the reversible dissociation of borate anions from the domain edge of the NiO_6 octahedra structure and a two-electron and three-proton equilibrium, followed by a chemical turnover-limiting step.[26] Our present study spectroscopically confirmed the report of Bediako et al. in that the active species functions at the domain edge of the NiO_6 octahedra structure. Thus, an increase in the number of NiO_6 domains is necessary to achieve an efficient OER catalyst.

The octahedra structures of transition-metal oxides (MnO_6, CoO_6, and NiO_6) are generally considered to exhibit high OER activity;[13−19,49−52] however, the direct spectroscopic detection of active octahedral species had not been achieved around the OER electrode potential. The XAFS technique used here has provided the first successful direct probing of the active species of Ni−B_i electrocatalyst during electrochemical reaction. This probing technique can be applied to many other OER electrocatalysts composed of transition-metal oxides such as Co−P_i,[16−19] Co−B_i,[17,18] nickel-glycine catalyst,[51] and MnO_x[49,50] to reveal the relationship between the active species and OER activity. The knowledge obtained by this study will be useful to develop more efficient water-splitting systems.

4. CONCLUSIONS

In summary, in situ O K-edge XAFS spectra were measured for a nickel−borate OER electrocatalyst. The XAFS peak was observed at 528.7 eV by changing the electrode potential for each sample, which demonstrates that higher order domains of the edge-sharing NiO_6 octahedra structure are generated at higher potentials. The upward potential dependence of the XAFS spectra resulted in an increase in the intensity of the absorption peak for the NiO_6 octahedra with the OER current. In contrast, the downward potential dependence of the XAFS spectra revealed that the NiO_6 peak remains even if the OER current is suppressed. The different behavior between the upward and downward potential sweeps indicates that water oxidation catalysis is likely to proceed at the domain edge of the NiO_6 octahedra. This is the first successful direct observation of active nickel oxide species reported for OER electrocatalysts.

■ ASSOCIATED CONTENT

Supporting Information

The Supporting Information is available free of charge on the ACS Publications website at DOI: 10.1021/acs.jpcc.5b06102.

Experimental procedures of in situ Ni K-edge XAFS, time course of current during electrodeposition and anodic oxidation, estimation of film thickness, in situ Ni K-edge XAFS spectra, and estimation of cation valence. (PDF)

■ AUTHOR INFORMATION

Corresponding Author

*Tel: +81-45-566-1592. Fax: +81-45-566-1697. E-mail: yoshida@chem.keio.ac.jp.

Notes

The authors declare no competing financial interest.

■ ACKNOWLEDGMENTS

This work using soft X-ray was performed at BL3U in the UVSOR Synchrotron of the Institute for Molecular Science (2014_206, 2013_603), and that using hard X-ray was performed at the Photon Factory (2014G539) and SPring-8 (2015A1138 and 2014A1058). This work was supported by Grants-in-Aid (nos. 22850015, 24750134, and 26248010) from the Japan Society for the Promotion of Science (JSPS), the Keio Gijuku Academic Development Fund, Keio Kogaku-kai Fund, and the Cooperative Research Program of the Catalysis Research Center of Hokkaido University (14A1004 and 15B1002). We thank K. Nitta and T. Ina in JASRI and T. Iida, M. Kawamura, M. Sasai, T. Yomogida, and N. Gon in Keio University for conducting the XAFS measurements.

■ REFERENCES

(1) Hisatomi, T.; Kubota, J.; Domen, K. Recent Advances in Semiconductors for Photocatalytic and Photoelectrochemical Water Splitting. *Chem. Soc. Rev.* **2014**, *43*, 7520−7535.

(2) Prévot, M. S.; Sivula, K. Photoelectrochemical Tandem Cells for Solar Water Splitting. *J. Phys. Chem. C* **2013**, *117*, 17879−17893.

(3) Osterloh, F. E. Inorganic Nanostructures for Photoelectrochemical and Photocatalytic Water Splitting. *Chem. Soc. Rev.* **2013**, *42*, 2294−2320.

(4) Yang, J.; Wang, D.; Han, H.; Li, C. Roles of Cocatalysts in Photocatalysis and Photoelectrocatalysis. *Acc. Chem. Res.* **2013**, *46*, 1900−1909.

(5) Tachibana, Y.; Vayssieres, L.; Durrant, J. R. Artificial Photosynthesis for Solar Water-splitting. *Nat. Photonics* **2012**, *6*, 511−518.

(6) Nocera, D. G. The Artificial Leaf. *Acc. Chem. Res.* **2012**, *45*, 767−776.

(7) Fujishima, A.; Honda, K. Electrochemical Photolysis of Water at a Semiconductor Electrode. *Nature* **1972**, *238*, 37−38.

(8) Luo, J.; Im, J.-H.; Mayer, M. T.; Schreier, M.; Nazeeruddin, M. K.; Park, N.-G.; Tilley, S. D.; Fan, H. J.; Grätzel, M. Water Photolysis at 12.3% Efficiency via Perovskite Photovoltaics and Earth-abundant Catalysts. *Science* **2014**, *345*, 1593−1596.

(9) Li, Y.; Zhang, L.; Torres-Pardo, A.; González-Calbet, J. M.; Ma, Y.; Oleynikov, P.; Terasaki, O.; Asahina, S.; Shima, M.; Cha, D.; et al. Cobalt Phosphate-modified Barium-doped Tantalum Nitride Nanorod Photoanode with 1.5% Solar Energy Conversion Efficiency. *Nat. Commun.* **2013**, *4*, 2566.

(10) Brillet, J.; Yum, J.-H.; Cornuz, M.; Hisatomi, T.; Solarska, R.; Augustynski, J.; Graetzel, M.; Sivula, K. Highly Efficient Water Splitting by a Dual-absorber Tandem Cell. *Nat. Photonics* **2012**, *6*, 824−828.

(11) Reece, S. Y.; Hamel, J. A.; Sung, K.; Jarvi, T. D.; Esswein, A. J.; Pijpers, J. J. H.; Nocera, D. G. Wireless Solar Water Splitting using Silicon-based Semiconductors and Earth-abundant Catalysts. *Science* **2011**, *334*, 645−648.

(12) Cox, C. R.; Lee, J. Z.; Nocera, D. G.; Buonassisi, T. Ten-percent Solar-to-fuel Conversion with Nonprecious Materials. *Proc. Natl. Acad. Sci. U. S. A.* **2014**, *111*, 14057−14061.

(13) Dincă, M.; Surendranath, Y.; Nocera, D. G. Nickel-borate Oxygen-evolving Catalyst that Functions under Benign Conditions. *Proc. Natl. Acad. Sci. U. S. A.* **2010**, *107*, 1337−1341.

(14) Surendranath, Y.; Bediako, D. K.; Nocera, D. G. Interplay of Oxygen-evolution Kinetics and Photovoltaic Power Curves on the

DOI: 10.1021/acs.jpcc.5b06102
J. Phys. Chem. C 2015, 119, 19279−19286

Construction of Artificial Leaves. *Proc. Natl. Acad. Sci. U. S. A.* **2012**, *109*, 15617−15621.
(15) Risch, M.; Klingan, K.; Heidkamp, J.; Ehrenberg, D.; Chernev, P.; Zaharieva, I.; Dau, H. Nickel-oxido Structure of a Water-oxidizing Catalyst Film. *Chem. Commun.* **2011**, *47*, 11912−11914.
(16) Kanan, M. W.; Nocera, D. G. In Situ Formation of an Oxygen-Evolving Catalyst in Neutral Water Containing Phosphate and Co^{2+}. *Science* **2008**, *321*, 1072−1075.
(17) Surendranath, Y.; Dincă, M.; Nocera, D. G. Electrolyte-Dependent Electrosynthesis and Activity of Cobalt-Based Water Oxidation Catalysts. *J. Am. Chem. Soc.* **2009**, *131*, 2615−2620.
(18) Esswein, A. J.; Surendranath, Y.; Reece, S. Y.; Nocera, D. G. Highly Active Cobalt Phosphate and Borate Based Oxygen Evolving Catalysts Operating in Neutral and Natural Waters. *Energy Environ. Sci.* **2011**, *4*, 499−504.
(19) Lutterman, D. A.; Surendranath, Y.; Nocera, D. G. A Self-Healing Oxygen-Evolving Catalyst. *J. Am. Chem. Soc.* **2009**, *131*, 3838−3839.
(20) Hong, Y.-R.; Liu, Z.; Al-Bukhari, S. F. B. S. A.; Lee, C. J. J.; Yung, D. L.; Chi, D.; Hor, T. S. A. Effect of Oxygen Evolution Catalysts on Hematite Nanorods for Solar Water Oxidation. *Chem. Commun.* **2011**, *47*, 10653−10655.
(21) Choi, S. K.; Choi, W.; Park, H. Solar Water Oxidation using Nickel-borate Coupled $BiVO_4$ Photoelectrodes. *Phys. Chem. Chem. Phys.* **2013**, *15*, 6499−6507.
(22) Pijpers, J. J.; Winkler, M. T.; Surendranath, Y.; Buonassisi, T.; Nocera, D. G. Light-induced Water Oxidation at Silicon Electrodes Functionalized with a Cobalt Oxygen-evolving Catalyst. *Proc. Natl. Acad. Sci. U. S. A.* **2011**, *108*, 10056−10061.
(23) Zhong, D. K.; Gamelin, D. R. Photoelectrochemical Water Oxidation by Cobalt Catalyst ("Co-Pi")/alpha-Fe_2O_3 Composite Photoanodes: Oxygen Evolution and Resolution of a Kinetic Bottleneck. *J. Am. Chem. Soc.* **2010**, *132*, 4202−4207.
(24) Bediako, D. K.; Lassalle-Kaiser, B.; Surendranath, Y.; Yano, J.; Yachandra, V. K.; Nocera, D. G. Structure-activity Correlations in a Nickel-borate Oxygen Evolution Catalyst. *J. Am. Chem. Soc.* **2012**, *134*, 6801−6809.
(25) Kanan, M. W.; Yano, J.; Surendranath, Y.; Dinca, M.; Yachandra, V. K.; Nocera, D. G. Structure and Valency of a Cobalt-phosphate Water Oxidation Catalyst Determined by In Situ X-ray Spectroscopy. *J. Am. Chem. Soc.* **2010**, *132*, 13692−13701.
(26) Bediako, D. K.; Surendranath, Y.; Nocera, D. G. Mechanistic Studies of the Oxygen Evolution Reaction Mediated by a Nickel−Borate Thin Film Electrocatalyst. *J. Am. Chem. Soc.* **2013**, *135*, 3662−3674.
(27) Surendranath, Y.; Kanan, M. W.; Nocera, D. G. Mechanistic Studies of the Oxygen Evolution Reaction by a Cobalt-phosphate Catalyst at Neutral pH. *J. Am. Chem. Soc.* **2010**, *132*, 16501−16509.
(28) Bediako, D. K.; Costentin, C.; Jones, E. C.; Nocera, D. G.; Savéant, J.-M. Proton−Electron Transport and Transfer in Electrocatalytic Films. Application to a Cobalt-Based O_2-Evolution Catalyst. *J. Am. Chem. Soc.* **2013**, *135*, 10492−10502.
(29) Risch, M.; Klingan, K.; Ringleb, F.; Chernev, P.; Zaharieva, I.; Fischer, A.; Dau, H. Water Oxidation by Electrodeposited Cobalt Oxides—Role of Anions and Redox-Inert Cations in Structure and Function of the Amorphous Catalyst. *ChemSusChem* **2012**, *5*, 542−549.
(30) Klingan, K.; Ringleb, F.; Zaharieva, I.; Heidkamp, J.; Chernev, P.; Gonzalez-Flores, D.; Risch, M.; Fischer, A.; Dau, H. Water Oxidation by Amorphous Cobalt-Based Oxides: Volume Activity and Proton Transfer to Electrolyte Bases. *ChemSusChem* **2014**, *7*, 1301−1310.
(31) Risch, M.; Shevchenko, D.; Anderlund, M. F.; Styring, S.; Heidkamp, J.; Lange, K. M.; Thapper, A.; Zaharieva, I. Atomic Structure of Cobalt-oxide Nanoparticles Active in Light-driven Catalysis of Water Oxidation. *Int. J. Hydrogen Energy* **2012**, *37*, 8878−8888.
(32) Du, P.; Kokhan, O.; Chapman, K. W.; Chupas, P. J.; Tiede, D. M. Elucidating the Domain Structure of the Cobalt Oxide Water Splitting Catalyst by X-ray Pair Distribution Function Analysis. *J. Am. Chem. Soc.* **2012**, *134*, 11096−11099.
(33) Farrow, C. L.; Bediako, D. K.; Surendranath, Y.; Nocera, D. G.; Billinge, S. J. L. Intermediate-Range Structure of Self-Assembled Cobalt-Based Oxygen-Evolving Catalyst. *J. Am. Chem. Soc.* **2013**, *135*, 6403−6406.
(34) Liu, Y.; Nocera, D. G. Spectroscopic Studies of Nanoparticulate Thin Films of a Cobalt-Based Oxygen Evolution Catalyst. *J. Phys. Chem. C* **2014**, *118*, 17060−17066.
(35) McAlpin, J. G.; Surendranath, Y.; Dinca, M.; Stich, T. A.; Stoian, S. A.; Casey, W. H.; Nocera, D. G.; Britt, R. D. EPR Evidence for Co(IV) Species Produced during Water Oxidation at Neutral pH. *J. Am. Chem. Soc.* **2010**, *132*, 6882−6883.
(36) Yoshida, M.; Iida, T.; Mineo, T.; Yomogida, T.; Nitta, K.; Kato, K.; Nitani, H.; Abe, H.; Uruga, T.; Kondoh, H. Electrochromic Characteristics of a Nickel Borate Thin Film Investigated by In Situ XAFS and UV/vis Spectroscopy. *Electrochemistry* **2014**, *82*, 355−358.
(37) Yoshida, M.; Yomogida, T.; Mineo, T.; Nitta, K.; Kato, K.; Masuda, T.; Nitani, H.; Abe, H.; Takakusagi, S.; Uruga, T.; et al. Photoexcited Hole Transfer to a MnO_x Cocatalyst on a $SrTiO_3$ Photoelectrode during Oxygen Evolution Studied by *In Situ* X-ray Absorption Spectroscopy. *J. Phys. Chem. C* **2014**, *118*, 24302−24309.
(38) Braun, A.; Sivula, K.; Bora, D. K.; Zhu, J.; Zhang, L.; Grätzel, M.; Guo, J.; Constable, E. C. Direct Observation of Two Electron Holes in a Hematite Photoanode during Photoelectrochemical Water Splitting. *J. Phys. Chem. C* **2012**, *116*, 16870−16875.
(39) Bora, D. K.; Braun, A.; Erat, S.; Ariffin, A. K.; Löhnert, R.; Sivula, K.; Töpfer, J. r.; Grätzel, M.; Manzke, R.; Graule, T.; et al. Evolution of an Oxygen Near-Edge X-ray Absorption Fine Structure Transition in the Upper Hubbard Band in α-Fe_2O_3 upon Electrochemical Oxidation. *J. Phys. Chem. C* **2011**, *115*, 5619−5625.
(40) Nagasaka, M.; Yuzawa, H.; Horigome, T.; Kosugi, N. In Operando Observation System for Electrochemical Reaction by Soft X-ray Absorption Spectroscopy with Potential Modulation Method. *Rev. Sci. Instrum.* **2014**, *85*, 104105.
(41) Nagasaka, M.; Yuzawa, H.; Horigome, T.; Hitchcock, A. P.; Kosugi, N. Electrochemical Reaction of Aqueous Iron Sulfate Solutions Studied by Fe L-Edge Soft X-ray Absorption Spectroscopy. *J. Phys. Chem. C* **2013**, *117*, 16343−16348.
(42) Kosugi, N.; Shigemasa, E.; Yagishita, A. High-Resolution and Symmetry-Resolved Oxygen K-edge Spectra of O_2. *Chem. Phys. Lett.* **1992**, *190*, 481−488.
(43) Doyle, C. S.; Kendelewicz, T.; Bostick, B. C.; Brown, G. E., Jr Soft X-ray Spectroscopic Studies of the Reaction of Fractured Pyrite Surfaces with Cr(VI)-containing Aqueous Solutions. *Geochim. Cosmochim. Acta* **2004**, *68*, 4287−4299.
(44) Gurevich, A. B.; Bent, B. E.; Teplyakov, A. V.; Chen, J. G. A NEXAFS Investigation of the Formation and Decomposition of CuO and Cu_2O Thin Films on Cu(100). *Surf. Sci.* **1999**, *442*, L971−L976.
(45) Gilbert, B.; Frazer, B. H.; Belz, A.; Conrad, P. G.; Nealson, K. H.; Haskel, D.; Lang, J. C.; Srajer, G.; De Stasio, G. Multiple Scattering Calculations of Bonding and X-ray Absorption Spectroscopy of Manganese Oxides. *J. Phys. Chem. A* **2003**, *107*, 2839−2847.
(46) Chen, J. G. NEXAFS Investigations of Transition Metal Oxides, Nitrides, Carbides, Sulfides and Other Interstitial Compounds. *Surf. Sci. Rep.* **1997**, *30*, 1−152.
(47) Burstein, G. T. A Hundred Years of Tafel's Equation: 1905−2005. *Corros. Sci.* **2005**, *47*, 2858−2870.
(48) Pandya, K. I.; O'Grady, W. E.; Corrigan, D. A.; McBreen, J.; Hoffman, R. W. Extended X-ray Absorption Fine Structure Investigations of Nickel Hydroxides. *J. Phys. Chem.* **1990**, *94*, 21−26.
(49) Robinson, D. M.; Go, Y. B.; Mui, M.; Gardner, G.; Zhang, Z.; Mastrogiovanni, D.; Garfunkel, E.; Li, J.; Greenblatt, M.; Dismukes, G. C. Photochemical Water Oxidation by Crystalline Polymorphs of Manganese Oxides: Structural Requirements for Catalysis. *J. Am. Chem. Soc.* **2013**, *135*, 3494−3501.
(50) Huynh, M.; Bediako, D. K.; Nocera, D. G. A Functionally Stable Manganese Oxide Oxygen Evolution Catalyst in Acid. *J. Am. Chem. Soc.* **2014**, *136*, 6002−6010.

DOI: 10.1021/acs.jpcc.5b06102
J. Phys. Chem. C 2015, 119, 19279−19286

(51) Wang, D.; Ghirlanda, G.; Allen, J. P. Water Oxidation by a Nickel-Glycine Catalyst. *J. Am. Chem. Soc.* **2014**, *136*, 10198−10201.
(52) Ahn, H. S.; Bard, A. J. Surface Interrogation of CoPi Water Oxidation Catalyst by Scanning Electrochemical Microscopy. *J. Am. Chem. Soc.* **2015**, *137*, 612−615.

DOI: 10.1021/acs.jpcc.5b06102
J. Phys. Chem. C 2015, 119, 19279−19286